Int. J. Heat Mass Transfer. Vol. 23, pp. 253–268
© Pergamon Press Ltd. 1980. Printed in Great Britain

0017-9310/80/0301-0253 $02.00/0

THEORY OF CONVECTIVE DROPLET VAPORIZATION WITH UNSTEADY HEAT TRANSFER IN THE CIRCULATING LIQUID PHASE

S. PRAKASH and W. A. SIRIGNANO

Department of Mechanical and Aerospace Engineering,
Princeton University, Princeton, NJ 08540, U.S.A.

(*Received* 27 *November* 1978 *and in revised form* 21 *May* 1979)

Abstract — The problem of liquid droplet vaporization in a hot convective gaseous environment is analyzed. A new gas-phase viscous, thermal and species concentration boundary layer analysis is developed using an integral approach. The gas-phase analysis is coupled with a modified form of a previous liquid-phase analysis for the internal motion and heat transfer [S. Prakash and W. A. Sirignano, *Int. J. Heat Mass Transfer* **21**, 885–895 (1978)]. The coupled problem is solved for three hydrocarbon fuels (*n*-hexane, *n*-decane, and *n*-hexadecane). The results show that the droplet vaporization is unsteady, and that the temperature distribution within the droplet is nonuniform for a significant part of the droplet lifetime. Some of the results are compared with the already existing correlations after correcting them for the heat flux into the liquid phase.

NOMENCLATURE

$a(\phi,\tau)$, as defined by equation (48);
a_0–a_4, coefficients of the gas-phase velocity profile;
A, strength of Hill's vortex;
$b(\phi,\tau)$, as defined by equation (48);
b_0–b_4, coefficients of the gas-phase density profile;
B, Spalding's transfer number;
c_0–c_4, coefficients of the fuel mass fraction profile;
C_2, as given by the boundary condition (i) of equation (47);
C_p, specific heat at constant pressure;
d, droplet diameter;
D, diffusion coefficient;
$g_1(\phi)$, dimensionless function as defined by equation (36);
$g_2(\phi)$, dimensionless function as defined by equation (44);
h, sensible enthalpy of the gaseous mixture;
h_i, total enthalpy including the chemical enthalpy of species i;
h_m, scale factor in m-direction as defined by equation (38);
h_ξ, scale factor in stream-wise direction;
h_ψ, scale factor in ψ-direction;
h_η, scale factor in the aximuthal direction;
L, heat of vaporization of the fuel;
L', modified heat of vaporization as defined by equation (17);
m, mass-weighted streamline coordinate defined by equation (35);
$\dot{m}_c$, mass vaporization rate with gas-phase convection;
$\dot{m}_{ss}$, mass vaporization rate with spherically symmetric vaporization;
$\dot{m}_s''$, vaporizing mass flux;
$\bar{\dot{m}}_s''$, average vaporizing mass flux;
M, Mach number;
M_i, molecular weight of ith species;
O( ), the order of ( );
p, pressure, also non-dimensional radius;
Pr, Prandtl number;
$\bar{q}''$, average heat flux;
r, radial distance in spherical polar coordinate system;
r_s, normal distance of the interface from the axis of symmetry;
R, droplet radius;
R, gas constant;
Re, Reynolds number based on radius;
Re_d, gas-phase Reynolds number based on diameter;
t, time;
T, temperature;
T_{av}, average temperature on a closed stream surface as defined by equation (41);
T_b, boiling point of the liquid;
T_e, temperature at the edge of gas-phase boundary layer;
T_0, initial temperature;
T_s, interface temperature;
u, gas-phase velocity in the x-direction;
u_e, velocity at the edge of gas-phase boundary layer;
u_s, tangential velocity at the interface;
U_∞, free stream gas-phase velocity relative to the droplet;
v, gas-phase velocity in the y-direction;
v_s, radial gas-phase velocity at the interface;
w_i, rate of production of the ith species;
x, gas-phase tangential coordinate;
y, gas-phase boundary layer coordinate normal to the interface;

Y_F, mass fraction of fuel;
Y_i, mass fraction of ith species.

Greek symbols

α, $= \lambda/\rho C_p$, thermal diffusivity;
δ, boundary layer thickness;
δ_1, δ_2, δ_H, δ_{Y_F}, the various gas-phase boundary layer thicknesses as defined by equations (a–d);
δ', as defined by equation (9a);
η, transformed boundary layer variable defined by equation (9); azimuthal direction in the spherical polar coordinates;
θ, tangential coordinate direction;
λ, thermal conductivity;
μ, viscosity;
ν, kinematic viscosity;
ξ, stream-wise coordinate direction;
ψ, stream function;
ϕ, dimensionless stream function defined by equation (33);
ρ, density;
τ, dimensionless time defined by equation (46);
τ_s, surface shear stress.

Subscripts

e, edge of the gas-phase boundary layer;
g, gas phase;
l, liquid phase;
n, non-dimensional quantities;
s, gas–liquid interface;
∞, free stream value;
0, initial value.

Superscripts

$'$, dimensionless quantities; differentiation with respect to x in the gas-phase boundary layer.

I. INTRODUCTION

THERE have been a number of studies of isolated liquid fuel droplet vaporization and combustion with spherical symmetry [1]. These studies have provided useful insights to the problem. However, many practical devices such as gas turbine or rocket combustors etc. involve droplet vaporization in a hot convective gaseous stream. Some semi-empirical correlations exist [2, 3, 4] which account for the convective motion in the gas phase and express the vaporization rate as a modification of the spherically symmetric case. These correlations are not very satisfactory, especially during the transient period of droplet heating [5].

In many practical high pressure combustors, the Reynolds number based upon the relative gas–droplet velocity is large [of O(100)] compared to unity for a significant part of the droplet lifetime [6]. This high Reynolds number in the gas phase has been demonstrated to imply that the shear stress at the gas–liquid interface is large enough to induce internal liquid-phase circulation [6, 7]. This liquid motion would be important in determining the heat and mass transfer (for the multicomponent fuel droplets) within the droplet and thereby would modify the vaporization rate.

The theoretical prediction of vaporization rate, including the liquid-phase convective motion, involves the solution of the coupled equations of motion, energy, and concentration in the gas and the liquid phases. The coupling between the conservation equations in the two phases occurs at the gas–liquid interface. The liquid-phase motion and the droplet heating were considered by the authors in a previous paper [7]. The liquid-phase problem was uncoupled from the gas phase by specifying the necessary interface conditions; it was shown that the droplet heating is unsteady and the temperature distribution is nonuniform for most of the droplet lifetime. In the present paper, the gas-phase boundary layer analysis is developed and coupled to the previous liquid-phase analysis which is modified to account for the changing droplet size due to vaporization. For the gas phase, an integral approach is used for the solution of the viscous, thermal and species concentration boundary layers.

The droplet vaporization problem with the gas–liquid coupling is solved for three hydrocarbon fuels, namely *n*-hexane, *n*-decane, and *n*-hexadecane, which provide a fairly wide range of volatility. The results showing the temporal variation of vaporization rate and the temperature distribution within the droplet are presented and discussed. Some of the results are compared with the already existing correlations for the droplet vaporization in a convective field.

In the next section the gas-phase analysis is developed. In Section III the results of the previous liquid-phase analysis [7] are summarized and the thermal core analysis is modified for the changing droplet radius. In Section IV the results of the coupled vaporization problem are presented and compared with some of the semi-empirical correlations already existing.

II. GAS-PHASE ANALYSIS

The gas-phase flow over a vaporizing droplet is essentially unsteady due to the temporal change in the size of the droplet. The characteristic time for changes in the gas phase is the residence time in the neighborhood of the droplet, and is of $O(d/U_\infty = 10\,\mu s)$ for a droplet of diameter 100 μm and in a free stream velocity of 10 m/sec. This time is much smaller than the droplet lifetime which is typically of O(5 msec) for a droplet of this size vaporizing in a convective field. Therefore, the quasi-steady gas-phase assumption can be employed. This assumption will be valid even at high ambient pressures in the convective vaporization case although it will not be so in the spherically-symmetric case.

For the gas-phase Reynolds number of O(100), the boundary layer approximation for the gas-phase flow can be employed with error in the boundary layer thickness of $O(Re^{-1/2})$. In this range of Reynolds number, for flow over a solid sphere, there is a recirculating wake in the rear stagnation-point region. The boundary layer approximation cannot represent the flow correctly in this region since the flow is essentially elliptic. However, the shear stress and the heat flux in the wake region are negligible for the Reynolds number of interest [8], so this region can be ignored in estimating the overall vaporization rate. For flow over a liquid droplet, the liquid motion will shift the point of zero shear stress towards the rear stagnation point thereby reducing the size of the wake and thus, the contribution of this region towards vaporization. Furthermore, the separation point where the surface velocity goes through zero would be aft of the zero stress point.

Although the conditions in a combustor are generally turbulent, since the typical size of a droplet [diameter of O(100 μm)] is much smaller than a typical large eddy size, a locally laminar boundary layer exists over the spherical droplet surface if the small distortion of the droplet which may exist at the Weber number of interest is neglected.

The conservation equations with axial symmetry in orthogonal boundary layer coordinates (see Fig. 1) for compressible flow over a sphere can be written neglecting the effect of curvature as follows [10]:

Continuity equation

$$\frac{\partial(\rho u r_s)}{\partial x} + \frac{\partial(\rho v r_s)}{\partial y} = 0. \tag{1}$$

Momentum equation in x-direction

$$\rho\left(u\frac{\partial u}{\partial x} + v\frac{\partial u}{\partial y}\right) = \rho_e u_e \frac{du_e}{dx} + \frac{\partial}{\partial y}\left(\mu\frac{\partial u}{\partial y}\right). \tag{2}$$

Energy equation

$$\rho\left(u\frac{\partial h}{\partial x} + v\frac{\partial h}{\partial y}\right) = \frac{\partial}{\partial y}\left(\lambda\frac{\partial T}{\partial y}\right) + \frac{\partial}{\partial y}\left[\rho\sum_{i=i}^{N}\left(D_i\frac{\partial Y_i}{\partial y}h_i\right)\right]. \tag{3}$$

Species equation

$$\rho\left(u\frac{\partial Y_i}{\partial x} + v\frac{\partial Y_i}{\partial y}\right) = \frac{\partial}{\partial y}\left(\rho D\frac{\partial Y_i}{\partial y}\right) \tag{4}$$

$$i = 1, 2, \ldots, N.$$

Equation of state

$$p = \left(\sum_{i=1}^{N}\frac{Y_i}{M_i}\right)\rho RT. \tag{5}$$

The normal distance of the droplet surface from the axis of symmetry is $r_s(x)$ and is given by

$$r_s(x) = R\sin\theta = R\sin(x/R). \tag{6}$$

In the above equations, radiation effects and the mass diffusion due to the temperature and pressure gradients have been neglected. Further simplification of the conservation equations was achieved by assuming that the specific heats C_{p_i} and the binary diffusion coefficients D_i of all the components are equal. The further assumptions were made that the Prandtl and Schmidt numbers in the gas phase are unity and that the kinetic energy is negligible compared to the sensible enthalpy which is true for small Mach numbers as in a combustor. The enthalpy h used in equation (3) represents the sensible enthalpy. The droplet is assumed to vaporize in a hot inert environment without chemical reaction.

The above system of conservation equations together with the appropriate boundary conditions and coupling with the liquid-phase equations form a complete set of equations to be solved for the gas-phase flow, and thence the vaporization rate can be determined. These gas-phase equations are all coupled to each other due to compressibility and due to vaporization and heat transfer at the gas–liquid interface. Further coupling with the liquid-phase equations of motion and energy to satisfy certain interface conditions complicates the situation.

However, to determine the vaporization rate in the hot environment, the details of the boundary layer profiles are not of so much interest as the heat and mass transfer, and the shear stress at the interface. Therefore, a simpler, integral approach is adopted for solving the gas-phase flow. The integral approach used is an extension of the Karman–Pohlhausen type of approach [10] in which the fourth degree polynomial profiles (for the pure vaporization problem which is considered here) are assumed for velocity, temperature, and concentration at any station along the flow. It is then necessary to satisfy certain boundary and interface conditions in addition to the integrated forms of the conservation equations. For the problem of pure vaporization considered here, it is sufficient to consider only the fuel conservation equation because the other species are treated as inert. On integrating equations

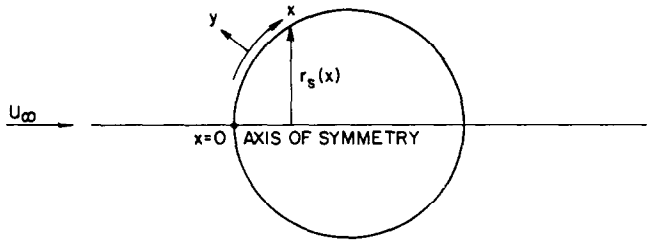

FIG. 1. Orthogonal boundary layer coordinate system.

(1–4) from $y = 0$ to $y = \delta$ (the thickness of the boundary layer which is assumed to be the same for momentum, energy and fuel species boundary layers), we obtain the integrated forms of the conservation equations

$$\frac{d\delta_2}{dx} + \frac{u_e'}{u_e}\left(2 + \frac{\delta_1}{\delta_2} + \frac{r_s' u_e}{r_s u_e'}\right)\delta_2 - \frac{(\rho v)_s}{\rho_e u_e}\left(1 - \frac{u_s}{u_e}\right) = \frac{\left(\mu \frac{\partial u}{\partial y}\right)_s}{\rho_e u_e^2} \quad (7a)$$

$$\frac{d\delta_H}{dx} + \frac{u_e'}{u_e}\left(1 + \frac{r_s' u_e}{r_s u_e'}\right)\delta_H - \frac{(\rho v)_s}{\rho_e u_e}\left(1 - \frac{h_s}{h_e}\right) = \frac{\left(\mu \frac{\partial h}{\partial y}\right)_s}{\rho_e u_e h_e} \quad (7b)$$

$$\frac{d\delta_{Y_F}}{dx} + \frac{u_e'}{u_e}\left(1 + \frac{r_s' u_e}{r_s u_e'}\right)\delta_{Y_F} - \frac{(\rho v)_s}{\rho_e u_e} Y_{Fs} = -\frac{\left(\mu \frac{\partial Y_F}{\partial y}\right)_s}{\rho_e u_e}, \quad (7c)$$

where the subscript s represents the value at the surface, and e represents the value at the outer edge of the boundary layer. Primes denote differentiation with respect to x. Notice the appearance of the surface velocities, u_s and v_s, due to liquid motion and vaporization, respectively, which do not appear for flow over a solid sphere in the absence of vaporization. The variables δ_1, δ_2, δ_H, and δ_{Y_F} appearing in the above equations represent the displacement, momentum, energy and fuel thicknesses, respectively, and are defined as integrals over the boundary layer thickness thus

$$\delta_1 = \int_0^\delta \left(1 - \frac{\rho u}{\rho_e u_e}\right) dy \quad (8a)$$

$$\delta_2 = \int_0^\delta \frac{\rho u}{\rho_e u_e}\left(1 - \frac{u}{u_e}\right) dy \quad (8b)$$

$$\delta_H = \int_0^\delta \frac{\rho u}{\rho_e u_e}\left(1 - \frac{h}{h_e}\right) dy \quad (8c)$$

$$\delta_{Y_F} = \int_0^\delta \frac{\rho u}{\rho_e u_e}(Y_F - Y_{Fe}) dy. \quad (8d)$$

A term

$$\left(\frac{1}{\rho_e}\frac{d\rho_e}{dx} \cdot \delta_2\right)$$

in the integrated momentum equation, and similar terms in the integrated energy and fuel equations have been dropped because they are of $O(M^2)$ for uniform ambient temperature and are very small compared to the other terms for $M \ll 1$ which is usually true for conditions in a combustor.

The various boundary layer thicknesses which have been defined above can be related to the boundary layer thickness $\delta(x)$ if the above integrals can be evaluated. It is convenient to define a transformed variable η related to y as

$$\eta = \frac{1}{\delta'(x)} \int_0^y \frac{\rho}{\rho_e} dy', \quad (9)$$

where

$$\delta'(x) = \int_0^{\delta(x)} \frac{\rho}{\rho_e} dy,$$

so that the interface $y = 0$ corresponds to $\eta = 0$, and the edge of the boundary layer $y = \delta(x)$ corresponds to $\eta = 1$. Polynomial profiles of fourth degree in η are assumed for velocity, density (or temperature), and fuel mass fraction. Therefore, let us assume that, in the boundary layer,

$$\frac{u}{u_e} = \sum_{n=0}^{4} a_n \eta^n \quad (10a)$$

$$\frac{\rho_e}{\rho} = \sum_{n=0}^{4} b_n \eta^n \quad (10b)$$

$$Y_F = \sum_{n=0}^{4} c_n \eta^n. \quad (10c)$$

Here, the coefficients a_n, b_n, c_n are functions of x and have to be determined. Such polynomial profiles cannot be assumed in the presence of a flame sheet because in that case the profiles will no longer be monotonically increasing or decreasing. The density ratio in the boundary layer can be related to the temperature ratio since the pressure across the boundary layer is constant, and if the gaseous mixture has a constant average molecular weight and obeys the perfect gas law, then

$$\frac{T}{T_e} = \frac{\rho_e}{\rho} = \sum_{n=0}^{4} b_n \eta^n. \quad (11)$$

The sensible enthalpy ratio can also be related to the density ratio by assuming that specific heat C_p is constant in the boundary layer; this is a reasonable assumption as more fuel with a higher C_p is present near the surface where temperature is lower, and so has an opposing effect on C_p variation due to composition and temperature. This constant C_p also provides a great simplification because now the enthalpy can be expressed as

$$\frac{h}{h_e} = \frac{T - T_0}{T_e - T_0} = \frac{1}{(1 - T_r)}\left(\sum_{n=0}^{4} b_n \eta^n - T_r\right), \quad (12)$$

where $T_r = T_0/T_e$ is constant since T_e does not vary much with x for small Mach number.

The coefficients a_n, b_n, and c_n, $(n = 0, 1, \ldots 4)$ are to be determined by use of the boundary conditions and of the integrated conservation equations. The boundary conditions imposed on the velocity, temperature, and fuel mass fractions profiles are as follows:

At the gas–liquid interface, i.e. at $\eta = 0$, or $y = 0$,

$$u = u_s(x),\ T = T_s(x),\ Y_F = Y_{F_s}(x). \quad (13)$$

At the outer edge of the boundary layer, i.e. at $\eta = 1$, or $y = \delta(x)$,

$$u = u_e(x), \frac{\partial u}{\partial y} = \frac{\partial^2 u}{\partial y^2} = 0; \tag{14a}$$

$$T = T_e, \frac{\partial T}{\partial y} = 0; \tag{14b}$$

$$Y_F = 0, \frac{\partial Y_F}{\partial y} = 0. \tag{14c}$$

In the boundary condition at the interface, Y_{F_s} is related to T_s through phase equilibrium. The quantities u_s, T_s, Y_{F_s}, at the interface are to be determined from the solution of the liquid-phase equations of motion and energy. For the gas-phase flow problem, these quantities are assumed to be known. Part of the coupling between the gas- and liquid-phase equations appears through these quantities.

The boundary condition at the edge of the boundary layer requires that the velocity, temperature, and fuel mass fraction profiles match smoothly to the outside flow. Therefore, the first two derivatives for velocity, and the first derivatives for temperature and fuel mass fraction are set equal to zero. The values of velocity, temperature, and fuel mass fraction at the edge of the boundary layer are assumed to be known. Here, it is assumed that there is no fuel present in the free stream, although the analysis could be developed with the fuel present without any great difficulty. This may be the situation in a combustor or part of it where fuel rich mixture is present and vaporization takes place under these conditions. The velocity distribution outside the boundary layer is assumed to be the potential flow over a sphere. The velocity field outside the boundary layer for flow over a solid sphere is not a potential flow mainly due to boundary layer separation upstream of the rear stagnation point; however, for flow over a liquid sphere, the liquid motion moves the zero-shear-stress point downstream of the corresponding point on the solid sphere. There is liquid motion in the downstream direction even beyond this point. Therefore, in the absence of any knowledge about the pressure or velocity fields outside the boundary layer, and without the elliptic flow problem being solved, the velocity can be approximated to the potential flow velocity. This approximation is better for flow over a liquid sphere than for flow over a solid sphere. Therefore, $u_e(x)$ can be expressed as

$$u_e(x) = \frac{3}{2} U_\infty \sin\left(\frac{x}{R}\right),$$

where U_∞ is the free stream velocity far upstream.

In addition to the above boundary conditions, it is required that the original conservation equations (1–4) be satisfied at the interface $y = 0$. This condition provides the following relations:

$$\frac{(\rho u)_s}{\rho_e u_e}\left(\frac{\partial u}{\partial x}\right)_{y=0} + \frac{(\rho v)_s}{\rho_e u_e}\left(\frac{\partial u}{\partial y}\right)_{y=0} = \frac{du_e}{dx} + \frac{1}{\rho_e u_e}\left[\frac{\partial}{\partial y}\left(\mu\frac{\partial u}{\partial y}\right)\right]_{y=0} \tag{15a}$$

$$(\rho u)_s\left(\frac{\partial h}{\partial x}\right)_{y=0} + (\rho v)_s\left(\frac{\partial h}{\partial y}\right)_{y=0} = \left[\frac{\partial}{\partial y}\left(\mu\frac{\partial h}{\partial y}\right)\right]_{y=0} \tag{15b}$$

$$(\rho u)_s\left(\frac{\partial Y_F}{\partial x}\right)_{y=0} + (\rho v)_s\left(\frac{\partial Y_F}{\partial y}\right)_{y=0} = \left[\frac{\partial}{\partial y}\left(\mu\frac{\partial Y_F}{\partial y}\right)\right]_{y=0}. \tag{15c}$$

Additional coupling between the gas and liquid phases is obtained because of the conservation of fuel mass flux and heat flux at the interface. These conservation conditions can be expressed as

$$\left(\rho D\frac{\partial Y_F}{\partial y}\right)_s = (\rho v)_s(Y_{F_s} - 1) \tag{16}$$

$$\left(\frac{\lambda}{C_p}\frac{\partial h}{\partial y}\right)_{s,g} = (\rho v)_s L + \left(\lambda\frac{\partial T}{\partial y}\right)_{s,l} \equiv (\rho v)_s L', \tag{17}$$

where L' as defined above includes the latent heat of vaporization and the heat flux into the liquid, which will be non-zero and positive, then not all the heat goes to vaporize the liquid. The subscripts g and l above refer to the gas phase and liquid phase, respectively. The assumption that Prandtl and Schmidt numbers are unity has been made earlier, therefore

$$D = \frac{\lambda}{C_p} = \mu$$

can be used in the above relations. The two conservation conditions, (16) and (17), also provide the coupling between the temperature and the fuel mass fraction profiles in the boundary layer.

Now we can look at all the unknowns and the boundary and interface conditions that are available. For the velocity profile, we have the five unknown coefficients, a_0 to a_4, to be determined. In addition to these, we have $\delta(x)$, the boundary layer thickness to be determined. Although $\delta(x)$ appears in the integrated energy and fuel conservation equations through δ_H and δ_{Y_F}, it will be treated as an unknown for the velocity profile realizing that all the equations are coupled. For these six unknowns, we have five boundary conditions given by equations (13), (14a), and (15a), and one ordinary differential equation given by (7a) to be satisfied. For the density or temperature profile, we have five coefficients, b_0 to b_4, and L' the total heat flux per unit mass, as the six unknowns. Correspondingly, there are four boundary conditions given by (13), (14b), and (15b), one interface constraint given by (17), and one ordinary differential equation (7b) to be satisfied. The fuel mass fraction profile has the five coefficients, c_0 to c_4, and $(\rho v)_s$ or v_s, which represents the vaporizing mass flux, as the six unknowns. The corresponding four boundary conditions are given by (13), (14) and (15c), one interface constraint is given by (16), and the ordinary differential equation is given by (7c). Thus the system of unknowns and boundary conditions and interface constraints along with the ordinary differential equations is complete and can be solved. However, it should be realized

that the profiles for velocity, temperature, etc., cannot be solved independently since the system of equations is coupled. It will be possible to eliminate many unknown coefficients through the algebraic relations which express the boundary conditions. This is briefly explained and the important variables to be resolved are outlined in the following.

To proceed further, it is necessary to change from y to η for the various integrals and the boundary conditions. The relation between η and y is given by equation (9). The thicknesses δ_1, δ_2, δ_H, and δ_{Y_F} can now be expressed in terms of integrals over η-domain and they can be related to $\delta(x)$ as follows:

$$\frac{\delta_1}{\delta'} = \int_0^1 \left(\frac{\rho_e}{\rho} - \frac{u}{u_e}\right) d\eta \tag{18a}$$

$$\frac{\delta_2}{\delta'} = \int_0^1 \frac{u}{u_e}\left(1 - \frac{u}{u_e}\right) d\eta \tag{18b}$$

$$\frac{\delta_H}{\delta'} = \int_0^1 \frac{u}{u_e}\left(1 - \frac{h}{h_e}\right) d\eta \tag{18c}$$

$$\frac{\delta_{Y_F}}{\delta'} = \int_0^1 \frac{u}{u_e} Y_F \, d\eta, \tag{18d}$$

where $\delta'(x)$ used above is related to $\delta(x)$ as given after equation (9). The quantities in the integrals are polynomials in η as given by (10) and (14), and thus the integrals can be evaluated in terms of the unknown coefficients of the polynomials. Similarly, the conditions at the interface given by (15) are transformed from y to η. Now the further assumption is made that the product $\rho\mu$ is constant across the boundary layer implying that μ is directly proportional to T in the boundary layer. Therefore

$$\rho\mu = \rho_e \mu_e \tag{19}$$

which may be a function of x. The various quantities are non-dimensionalized and written with subscript n as follows:

$$x_n = \frac{x}{R}\,;\; u_n = \frac{u}{U_\infty}\,;\; u_{en} = \frac{u_e}{U_\infty} = \frac{3}{2}\sin x_n. \tag{20}$$

Defining $Re_g = U_\infty R/\nu_e$, and non-dimensionalizing the quantities of the order of boundary layer thickness with $(Re_g)^{1/2}$ gives

$$\begin{aligned} \delta_n' &= \frac{\delta'}{R}(Re_g)^{1/2} \\ \delta_{2n} &= \frac{\delta_2}{R}(Re_g)^{1/2} \\ v_{sn} &= \frac{v_s}{U_\infty}(Re_g)^{1/2}. \end{aligned} \tag{21}$$

Similarly, δ_1, δ_H, and δ_{Y_F} are non-dimensionalized. L' is non-dimensionalized as

$$L_n' = L'/h_e.$$

Since $r_s x_n = R \sin x_n$, then

$$\frac{1}{r_s}\frac{dr_s}{dx}\frac{u_e}{du_e/dx} = 1. \tag{22}$$

By use of equation (19) and the above non-dimensionalized quantities, the boundary conditions and the differential equations after some algebraic manipulation can be written as below.

The integrated momentum, energy and fuel conservation equations (7a–c) now become

$$\frac{d\delta_{2n}}{dx_n} + \frac{1}{\sin x_n}[\cos x_n(3 + \delta_{1n}/\delta_{2n})\delta_{2n} - 2v_{sn}(1 - a_0)/3b_0 - 2a_1/3\delta_n'] = 0 \tag{23a}$$

$$\frac{d\delta_{Hn}}{dx_n} + \frac{1}{\sin x_n}\{2(\cos x_n)\delta_{Hn} - 2v_{sn}[(1 - b_0)/(1 - T_r) + L_n']/3b_0\} = 0 \tag{23b}$$

$$\frac{d\delta_{Y_{Fn}}}{dx_n} + \frac{2}{\sin x_n}[(\cos x_n)\delta_{Y_{Fn}} - v_{sn}/3b_0] = 0. \tag{23c}$$

The relation between the temperature gradient at the interface (expressed by b_1) and the heat flux L_n', and the relation between the fuel mass fraction gradient at the interface (expressed by c_1) and the vaporizing mass flux v_{sn} are obtained from the conservation of energy and fuel mass fraction at the interface as given by equations (16) and (17), respectively. These relations are

$$b_1 = v_{sn}\delta_n' L_n'(1 - T_r)/b_0, \tag{24}$$

where

$$\begin{aligned} T_r &= T_0/T_e \\ c_1 &= v_{sn}\delta_n(c_0 - 1)/b_0. \end{aligned} \tag{25}$$

Similarly, the relation between a_2 and δ_n', between b_2 and b_1, and between c_2 and c_1 are obtained from the relations (15a–c) which have been developed by requiring that the conservation equations be satisfied at the interface. The coefficients $a_0(x)$, $b_0(x)$, and $c_0(x)$ which express the tangential velocity, the temperature, and the fuel mass fraction at the interface are assumed to be known from the liquid-phase analysis and provide the coupling between the two phases requiring an iterative solution for the coupled problem. The other coefficients of the polynomial profiles, such as a_1, a_3, a_4, b_3, b_4, c_3, and c_4 can be expressed in terms of the coefficients a_0, a_2, b_0, b_1, b_2, c_0, c_1, and c_2, respectively through linear algebraic relations. The details of these relations and other algebraic details are given in [9]. In addition to these algebraic relations, the quantities δ_{1n}, δ_{2n}, δ_{Hn}, $\delta_{Y_{Fn}}$ are related to $\delta_n'(x)$ through the integrals given by equations (18a–d).

Summarizing, we can say that the unknown quantities to be solved from the coupled nonlinear ordinary differential equations (23a–c) are $\delta_n'(x)$, $L_n'(x)$ and $v_{sn}(x)$. Once these quantities are known, shear stress, heat flux, and mass vaporization rate can be calculated

using simple algebraic relations [9]. Instead of v_{sn} as the dependent variable, non-dimensional mass flux rate was chosen as the dependent variable which is related to v_{sn} by

$$\dot{m}''_{sn} = \frac{v_{sn}}{b_0} = \frac{\rho_s}{\rho_e} v_{sn}. \tag{26}$$

Similarly, $b_1(x)$ which is related to L'_n by equation (24) was chosen as the dependent variable for convenience in algebraic manipulation. Shear stress can be easily calculated from δ'_n thus:

$$\frac{\tau_s}{\rho_\infty U_\infty^2}(Re_g)^{1/2} = \frac{3}{2}\sin x_n \frac{a_1}{\delta'_n}, \tag{27}$$

where a_1 is related to δ'_n through known algebraic relations. Heat flux into the liquid can be determined by taking the difference of total heat flux and the latent heat flux for vaporization, so

$$\frac{1}{h_e}\left(\lambda \frac{T}{y}\right)_{s,l} = L'_n - \frac{L}{h_e}. \tag{28}$$

After substantial algebraic manipulation [9], the ordinary differential equations (23a–c) can be written with δ'_n, $\dot{m}''_{sn}$ and b_1 as the dependent variables. The forms of these equations, dropping the subscript n for the non-dimensional quantities for convenience, are

$$\frac{d\delta'}{dx} = \frac{1}{\sin x} f_1(x, \delta', b_1, \dot{m}''_s) = F_1(x, \delta', b_1, \dot{m}''_s) \tag{29a}$$

$$\frac{d\dot{m}''_s}{dx} = \frac{1}{\sin x} f_2\left(x, \delta', b_1, \dot{m}_s, \frac{d\delta'}{dx}\right) = F_2\left(x, \delta', b_1, \dot{m}''_s, \frac{d\delta'}{dx}\right) \tag{29b}$$

$$\frac{db_1}{dx} = \frac{1}{\sin x} f_3\left(x, \delta', b_1, \dot{m}''_s, \frac{d\delta'}{dx}, \frac{d\dot{m}''_s}{dx}\right) = F_3\left(x, \delta', b_1, \dot{m}''_s, \frac{d\delta'}{dx}, \frac{d\dot{m}''_s}{dx}\right). \tag{29c}$$

The functional forms of f_1, f_2, f_3 are very long [9]. In general, these functions are nonlinear. The equations (29a–c) are coupled nonlinear ordinary differential equations and have to be solved simultaneously.

To start the solution of these equations, solution at some value of x is required. It can be seen that at $x = 0$ (i.e. at the forward stagnation point), the right-hand sides of the equations should go to infinity unless the multiplying functions are zero. So it is required that at $x = 0$,

$$f_1 = 0, \quad f_2 = 0, \quad f_3 = 0, \tag{30}$$

and these conditions provide the starting solution at the front stagnation point. Now the right-hand sides of equations (29a–c) are indeterminate, so use is made of symmetry at $x = 0$ which requires that the gradients be zero. Thus, at $x = 0$

$$\frac{d\delta'}{dx} = 0, \quad \frac{db_1}{dx} = 0, \quad \frac{d\dot{m}''_s}{dx} = 0. \tag{31}$$

With these starting conditions, equations (29a–c) are integrated numerically moving forward in the x-direction; the integration is conducted until the zero-shear-stress point is reached. Beyond this point the boundary layer becomes very thick, disallowing the boundary layer approximation, and the shear stress and heat and mass fluxes are small in this region for the Reynolds number of interest.

The gas-phase problem formulated here can be uncoupled from the liquid-phase equations of motion and energy if the surface velocity and temperature are specified and the droplet radius is assumed to be constant. However, in the coupled problem, the liquid-phase problem is solved to get the surface velocity and temperature which are then used as input for the gas-phase problem. But since the liquid-phase solution depends on the gas-phase solution due to shear stress and heat flux at the interface, an iterative solution of the coupled problem is required.

For the numerical integration of equations (29a–c), first the stagnation-point solution was obtained by solving the system of nonlinear coupled algebraic equations (30). These equations were solved numerically using the Newton–Raphson technique for achieving faster convergence to the solution. The stagnation-point solution was utilized for $x \leq x_0$, which is taken to be five steps in the x-direction where each step equals 0.02. Once this solution was obtained, a marching procedure was employed for the solution of the differential equations (29a–c) for $x > x_0$. The equations (29a–c) were integrated using an explicit third-order Runge–Kutta scheme [9]. Solution for the uncoupled gas-phase problem was obtained for a particular case of ethyl alcohol in air at 1000 K at 20 atm. The values of u_s/u_e, and T_s were assumed to be constant at the interface, although they will vary with x in the coupled problem. The values chosen for these quantities were

$$u_s/u_e = 0.1, \quad T_s = 353\,\text{K}.$$

The results of the calculations are shown in Fig. 2. It can be seen from the figure that the non-dimensional shear stress first increases, reaches a maximum, and then decreases to zero at about 2.0 radians from the front stagnation point. The heat and the vaporizing mass fluxes continually decrease in the downstream direction due to the increasing boundary layer thickness, and are of the order of 20% of their front stagnation region values near the zero-shear-stress point. These quantities will remain small beyond the zero-shear-stress point for the Reynolds number of interest, and will be neglected in the present analysis. It should be noted that the heat flux into the liquid phase is more than 80% of the total heat flux at this specified value of the surface temperature. However, as the surface becomes heated with time, the fraction of the total heat flux into the liquid phase will decrease. As we shall see later from the solution of the coupled unsteady problem, this fraction stays at a significant value and therefore the unsteady state vaporization

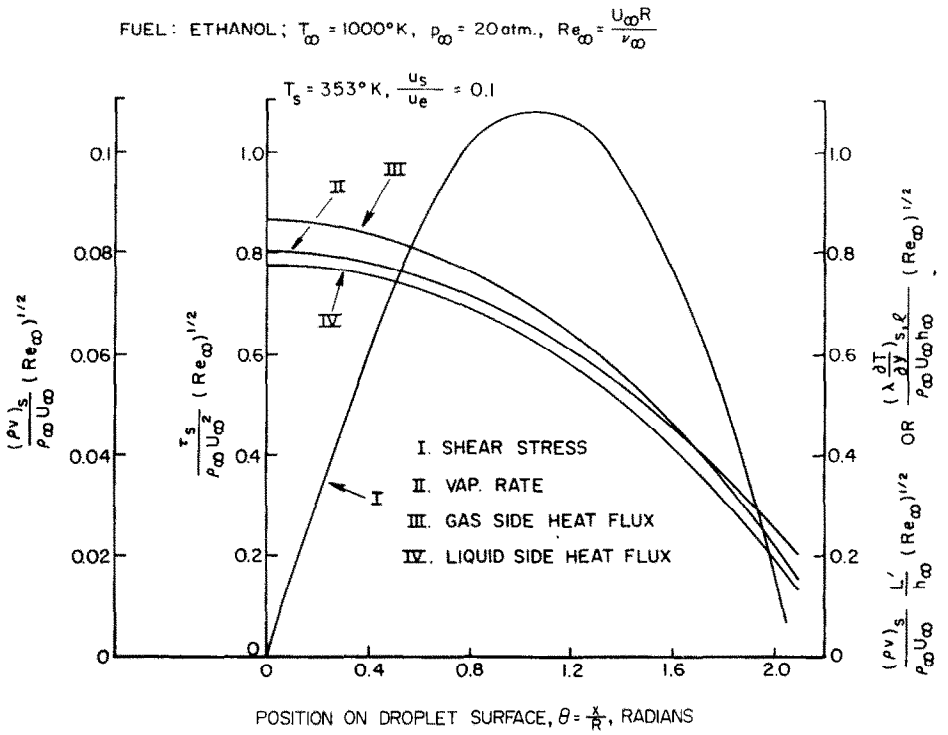

FIG. 2. Comparison of results in this paper with available experimental results.

persists for a large part of the droplet lifetime.

III. LIQUID-PHASE ANALYSIS

The liquid-phase analysis was performed in a previous paper [7] and the reader is referred to that for the details. The results of that analysis will be summarized here, and the analysis for the thermal core will be modified to account for the decreasing droplet radius. In the uncoupled liquid-phase analysis, it was shown [7] that the liquid motion is quasi-steady and consists of a Hill's vortex in the droplet core with a thin viscous boundary layer near the droplet surface and an inviscid internal wake near the axis of symmetry. In the viscous boundary layer, the velocity perturbations are small although the vorticity perturbations are large. Similarly, there is a thin quasi-steady thermal boundary layer near the droplet surface in which the temperature gradients are large. The analysis of the thermal boundary layer is similar to that of the viscous boundary layer and is coupled to the thermal core in the matching region.

The droplet core heating was shown to be essentially unsteady and normal to the closed streamlines* because of a very short residence time along a streamline compared to the droplet lifetime. Therefore, the orthogonal streamline coordinates were used for the energy equation in the core. However, for a vaporizing droplet where the radius is decreasing, the closed stream surfaces cannot retain their shape and size and have to deform to adjust to the decreasing radius in time. Since the liquid motion is quasi-steady, this change takes place in a very short time, and at any instant we have closed Hill's vortex streamlines. The mass which vaporizes in any infinitesimal time period is taken to be all of the liquid between the droplet surface and a neighboring liquid stream surface at the beginning of that time period. Therefore, the mass associated with the center of the vortex, which remains coldest, vaporizes only at the end. This suggests the use of orthogonal mass weighted streamline coordinates for the energy equation in the core when the droplet radius is decreasing.

The stream function for the Hill's vortex is redefined so that the center of the vortex corresponds to the zero value of ψ,

$$\psi = AR^4/8 - Ar^2(R^2 - r^2)\sin^2\theta/2. \quad (32)$$

A non-dimensional stream function ϕ is defined such that its value is zero at the vortex center and unity at the droplet surface so

$$\phi = 8\psi/AR^4 = 1 - 4p^2(1 - p^2)\sin^2\theta, \quad (33)$$

where $p = r/R$.

In the orthogonal streamline coordinate system (ξ, ψ, η), η being in the azimuthal direction, the cor-

*The axisymmetric stream surfaces will be referred to as streamlines.

responding scale factors are

$$h_\xi = Ar^5 u_1 \cos^5\theta/2$$
$$h_\psi = 1/(ru_1 \sin\theta) \quad (34)$$
$$h_\eta\, r\sin\theta,$$

so that $h_\psi h_\eta = 1/u_1$, where u_1 is the only velocity component in the streamwise direction ξ.

A quantity m, proportional to the mass contained within any closed stream surface, can now be written as

$$m(\psi) = \int_0^\psi \oint_{\psi=\text{constant}} h_\psi h_\eta h_\xi \,\mathrm{d}\xi\,\mathrm{d}\psi. \quad (35)$$

The above quantity can be expressed in terms of the non-dimensional stream function ϕ, noting that $h_\psi h_\eta = 1/u_1$, and defining a dimensionless function of ϕ as follows:

$$\oint_{\substack{\psi=\text{constant}\\ \phi=\text{constant}}} \frac{h_\xi \mathrm{d}\xi}{u_1} = \frac{8}{AR} q_1(\phi). \quad (36)$$

Now m, which is a function of ϕ and t, becomes

$$m(\phi, t) = R^3 \int_0^\phi g_1(\phi)\mathrm{d}\phi. \quad (37)$$

The time dependence appears through the radius of the droplet which is decreasing, and $g_1(\phi)$ is defined by equation (36).

The orthogonal mass-weighted streamline coordinate system that should be used for the energy equation in the thermal core is (ζ, m, η) as explained earlier. The scale factor associated with the m-coordinate is

$$h_m = \frac{AR}{8g_1(\phi)} \cdot h_\psi. \quad (38)$$

In this coordinate system, there is only one component of velocity u_1 in the stream-wise direction at any instant. The energy equation with axial symmetry in this coordinate system is

$$\frac{\partial T}{\partial t} + \frac{u_1}{h_\xi}\frac{\partial T}{\partial \xi} = \frac{\alpha_l}{h_\xi h_m h_\eta}\left[\frac{\partial}{\partial \xi}\left(\frac{h_m h_\eta}{h_\xi}\frac{\partial T}{\partial \xi}\right) + \frac{\partial}{\partial m}\left(\frac{h_\eta h_\xi}{h_m}\frac{\partial T}{\partial m}\right)\right] \quad (39)$$

Since the temperature along any closed contour, m = constant, is assumed uniform at any instant because of a rapid recirculation, the coordinate ξ can be formally eliminated from the energy equation by integrating it along this closed contour. Multiplying throughout by u_1, noting that $h_\psi h_\eta = 1/u_1$, and integrating the above equation along a closed contour, m = constant, we notice that the second term on the left-hand side and first term on the right-hand side vanish because of the continuity of T and

$$\left(\frac{h_m h_\eta}{h_\xi}\frac{\partial T}{\partial \xi}\right)$$

in the flow field. The energy equation now simplifies to

$$\oint_{m=\text{constant}} \frac{1}{u_1}\frac{\partial T}{\partial t} h_\xi \mathrm{d}\xi = \alpha_l \oint_{m=\text{constant}} \frac{8g_1}{AR}\frac{\partial}{\partial m}\left(\frac{h_\eta h_\xi}{h_m}\frac{\partial T}{\partial m}\right)\mathrm{d}\xi. \quad (40)$$

The above equation in (m, t) coordinates has a moving boundary since the value of m changes at the core boundary as the droplet vaporizes. Therefore, we change to (ϕ, t) in which the value of ϕ is constant at both the boundaries, i.e. at the center of the vortex and the core boundary. Before making the change of variable, we define an average temperature on a 'm = constant' contour (which is also a 'ϕ = constant' contour at any instant, although the value of ϕ changes with time) as

$$T_{\mathrm{av}}(m, t) = \oint \frac{T}{u_1} h_\xi \mathrm{d}\xi \Big/ \left[\oint \frac{h_\xi \mathrm{d}\xi}{u_1}\right]. \quad (41)$$

Now the contour integrations in the energy equation (40) can be changed to a 'ϕ = constant' contour at any instant, realizing that the velocity field, the droplet radius, and ϕ change very little for the corresponding 'm = constant' contour during the short residence time along such a contour. However, the time derivative on the left-hand side of the equation is still taken with m kept constant, since the change in average temperature on a 'm-constant' contour is on a time scale which is comparable to the lifetime of the droplet. Furthermore, we define the average temperature gradient on a closed contour as follows:

$$\oint \left(\frac{h_\eta}{h_\psi}\right)\frac{\partial T}{\partial \phi} h_\xi \mathrm{d}\xi = \frac{\partial T_{\mathrm{av}}}{\partial \phi}\oint \left(\frac{h_\eta}{h_\psi}\right) h_\xi \mathrm{d}\xi. \quad (42)$$

Now given the relations between h_m and h_ψ, and between m and ϕ, and the definitions of average temperature and its gradient as above, the energy equation (40) can be written in the (m, t) coordinate system as

$$\frac{\partial T_{\mathrm{av}}}{\partial t}\oint \frac{h_\xi \mathrm{d}\xi}{u_1} = \frac{8\alpha_l g_1}{AR}\frac{\partial}{\partial m}\left[\frac{\partial T_{\mathrm{av}}}{\partial m}\frac{8g_1}{AR}\oint \frac{h_\xi h_\eta}{h_\psi}\mathrm{d}\xi\right]. \quad (43)$$

Defining

$$g_1(\phi) = \frac{AR}{8}\oint \frac{h_\xi \mathrm{d}\xi}{u_1}$$

as given by (36), and

$$g_2(\phi) = \frac{8}{AR^5}\oint \left(\frac{h_\eta}{h_\psi}\right) h_\xi \mathrm{d}\xi, \quad (44)$$

and changing to the (ϕ, t) system, we can write the energy equation in the form

$$g_1(\phi)\frac{\partial T_{\mathrm{av}}}{\partial t} - \left[\frac{3}{R}\frac{\mathrm{d}R}{\mathrm{d}t}\int_0^\phi g_1(\phi')\mathrm{d}\phi'\right]\frac{\partial T_{\mathrm{av}}}{\partial \phi} = \frac{\alpha_l}{R^2}\frac{\partial}{\partial \phi}\left[g_2(\phi)\frac{\partial T_{\mathrm{av}}}{\partial \phi}\right]. \quad (45)$$

Temperature and time are non-dimensionalized thus

$$T'_{av} = \frac{T_{av} - T_0}{T_b - T_0}$$

$$\tau = \alpha_l t / R_0^2, \tag{46}$$

where R_0 is the initial radius of the droplet. The energy equation can now be written as

$$\frac{\partial T'_{av}}{\partial \tau} = a(\phi, \tau)\frac{\partial^2 T'_{av}}{\partial \phi^2} + b(\phi, \tau)\frac{\partial T'_{av}}{\partial \phi}, \tag{47}$$

where

$$a(\phi, \tau) = \frac{R_0^2}{R^2}\frac{g_2(\phi)}{g_1(\phi)},$$

and

$$b(\phi, \tau) = \frac{R_0^2}{R^2}\frac{\mathrm{d}[g_2(\phi)]}{\mathrm{d}\phi}\frac{1}{g_1(\phi)} + \frac{3}{R}\frac{\mathrm{d}R}{\mathrm{d}\tau}\cdot\int_0^{\phi} g_1 (\phi')\mathrm{d}\phi'/g_1(\phi). \tag{48}$$

The form of the energy equation (47) is identical to the one given by (26) in [7] except for the $\mathrm{d}R/\mathrm{d}\tau$ term in $b(\phi, \tau)$, and the (R_0^2/R^2) terms which appear due to the changes in the droplet radius. The boundary conditions to equation (47) are the same as in [7]. These are as follows:

(i) At the core boundary, i.e. $\phi = \phi_0$,

$$\frac{\partial T'_{av}}{\partial \phi} = C_2(t).$$

(ii) At the center of the vortex, i.e. at $\phi = 0$, the temperature is a regular function of ϕ, and therefore

$$\frac{\partial T'_{av}}{\partial \tau} = b(\phi, \tau) - \frac{\partial T'_{av}}{\partial \phi}.$$

(iii) In addition to these boundary conditions, the initial condition is that at $\tau = 0$,

$$T'_{av} = 0.$$

In the boundary condition (i) above, the temperature gradient $C_2(t)$ is obtained by requiring the continuity of heat flux in the matching region of the thermal boundary layer and the thermal core. The energy equation in the thermal core is solved numerically using a Crank–Nicholson type of scheme and the solution is marched forward in time, solving the gas-phase equations and the liquid-phase equations of motion, and thermal boundary layer equations at each instant.

IV. SOLUTION OF THE COUPLED PROBLEM, RESULTS AND DISCUSSION

In the coupled problem with vaporization, first the gas-phase boundary layer is solved using the initial guess or the relaxed previous iterated values for surface velocity U_s and the surface temperature T_s. With the shear stress and the heat flux from the gas-phase solution, the liquid-phase viscous and thermal boundary layers and then the thermal core are resolved. The gas-phase and liquid-phase solutions are iterated until the required convergence is achieved. The new droplet radius corresponding to the next time step is calculated and the process repeated at the advanced time. Since the droplet gets heated in time, the liquid viscosity and thus the strength of the Hill's vortex are updated in time. The calculations in time are continued until the square root of the droplet mass is 30% of the original value, implying that the droplet mass left is about 9% of the original mass. The details of the calculation procedure are given in [9].

The overall vaporization rate at any instant is calculated by integrating the vaporizing flux over the droplet surface. Therefore, the mass vaporization rate and the time rate of change of droplet radius at any instant can be expressed by

$$\frac{\mathrm{d}R}{\mathrm{d}t} = -\frac{1}{2\rho_l}\int_0^{\theta_s} \dot{m}''_s \sin\theta \,\mathrm{d}\theta, \tag{49}$$

where $\dot{m}''_s$ is the vaporizing mass flux and is integrated up until the zero-shear-stress point θ_s, since the contribution of the region beyond this point is small for the Reynolds number of interest and cannot be calculated with the boundary layer approximation.

The coupled problem was solved for three hydrocarbon fuels in air at 1000 K and 10 atm. The three fuels chosen were *n*-hexane, *n*-decane, and *n*-hexadecane to get a fairly wide range of volatility. The results of computation with these three fuels are plotted in Figs. 3–5 which show the variation of $(R/R_0)^{3/2}$ and the non-dimensional average vaporizing mass flux $(\bar{\dot{m}}''_s)$ scaled with the instantaneous gas-phase Reynolds number. This is a rational choice for presentation of the results since, in the limits of a quasi-steady, high-Reynolds-number system, $(R/R_0)^{3/2}$ is linear in time. Naturally, its derivative is constant in that limit. When the gas-phase Reynolds number is changing due to the droplet radius alone, as assumed in the present study, the average vaporizing mass flux is proportional to the derivative $(\mathrm{d}(R/R_0)^{3/2})/\mathrm{d}\tau$. As seen from the figures, the slope of the $(R/R_0)^{3/2}$ curve is initially small due to the small vaporization rate and the heating of the droplet. This slope and the average mass flux increase rather sharply for the more volatile fuel, *n*-hexane, and gradually for the less volatile fuels, *n*-decane and *n*-hexadecane. As the droplet gets heated, the change in average vaporizing mass flux is slower and tends towards an asymptotic value. The slope of the average mass flux curve is much smaller for *n*-hexane than for *n*-hexadecane towards the end. This behavior is also shown in Fig. 6 which shows the variation of droplet surface temperature at the $\theta = 90°$ point, and the temperature at the center of the vortex. The surface temperature rises sharply for the more volatile fuel, and later the change becomes smaller. Note that the surface temperature for each of the three fuels is less than the boiling point of the fuel (more so,

for the less volatile fuel) even at the end of the droplet lifetime. Here and in the following discussion, the end of the droplet lifetime will refer to the instant when $(R/R_0)^{3/2} = 0.3$ because more than 90% of the original mass has vaporized, and the computation is not carried on beyond this time. Note that the Reynolds number decreases only by a factor of about two up to this point, so that the high Reynolds number approximation remains valid throughout the calculation.

The temperature at the center of the vortex which is cold initially rises with time as seen from Fig. 6. The vortex center temperature is about 20°C lower for hexadecane and about 6°C lower for hexane, and in between the two for decane, even at the end of droplet lifetime. It is considerably lower than the droplet surface temperature during the earlier part of the lifetime. Therefore, the uniform temperature assumption seems to be inappropriate for most of the droplet lifetime.

Figure 7 shows the variation of non-dimensional average heat flux, scaled with instantaneous Reynolds number, with time for the three fuels. Similarly, Fig. 8

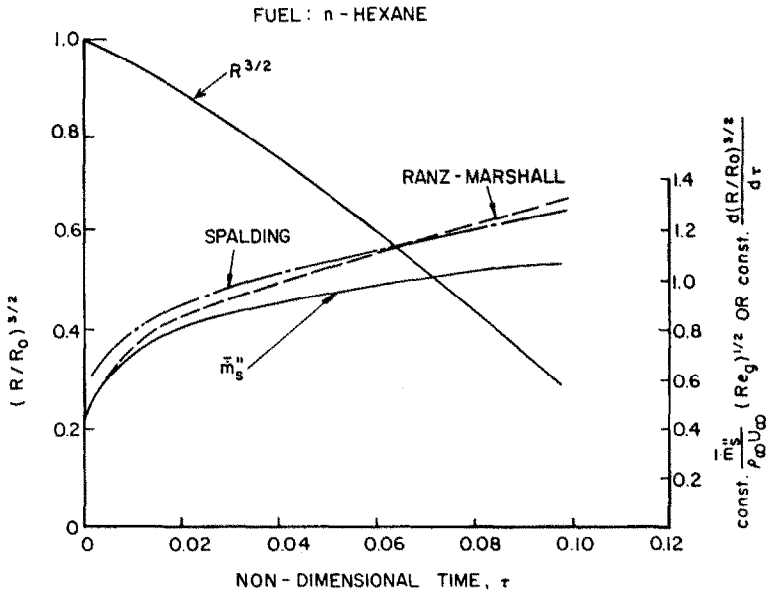

FIG. 3. Droplet size and vaporization rate vs time.

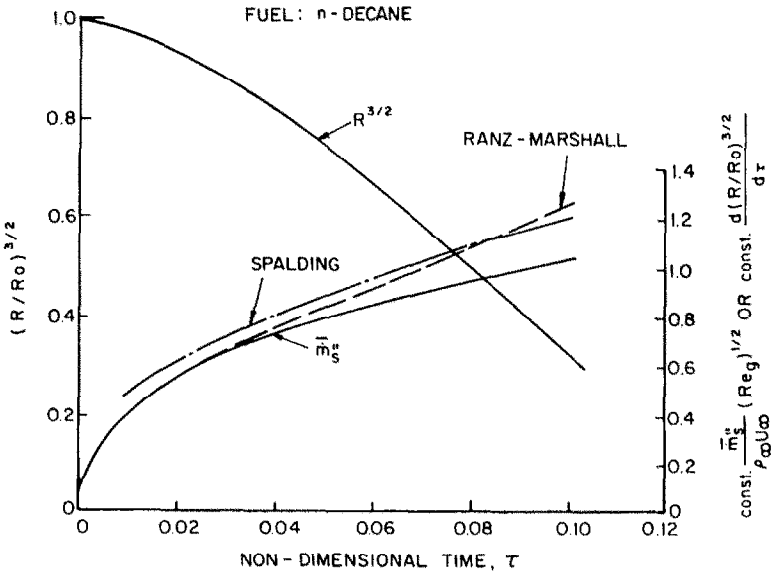

FIG. 4. Droplet size and vaporization rate vs time.

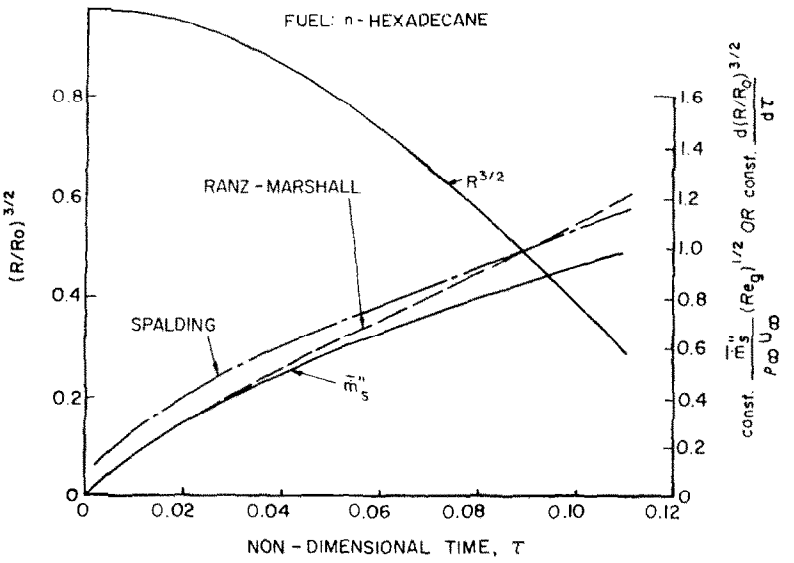

FIG. 5. Droplet size and vaporization rate vs time.

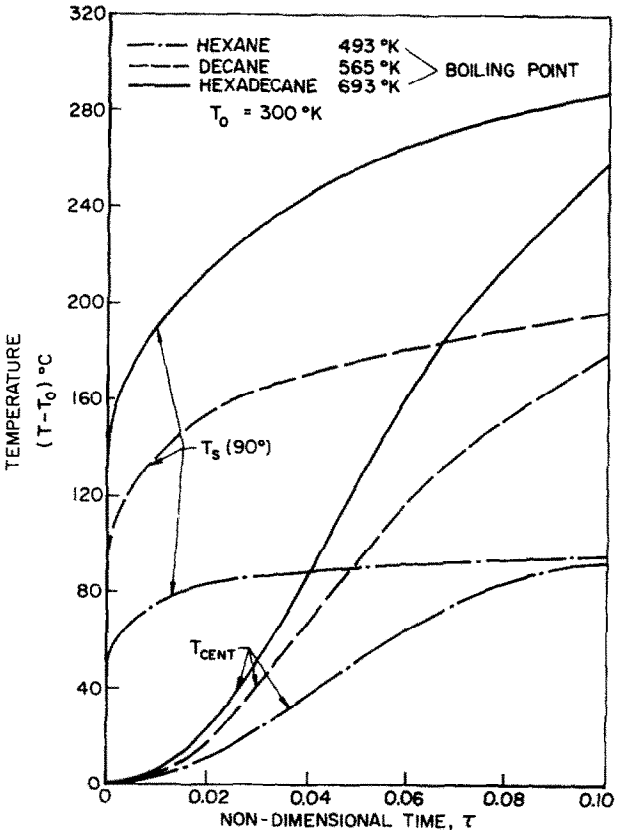

FIG. 6. Surface and vortex center temperature variation.

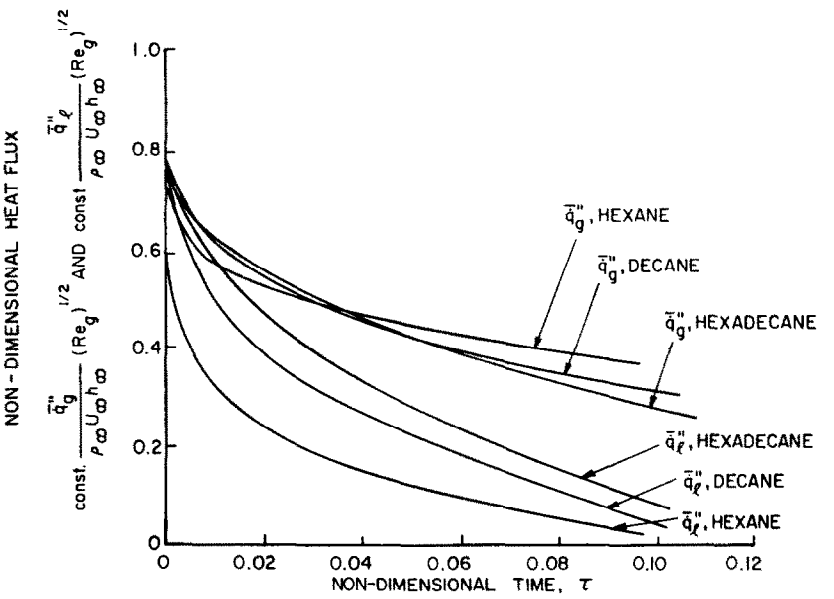

FIG. 7. Average heat flux for the three fuels.

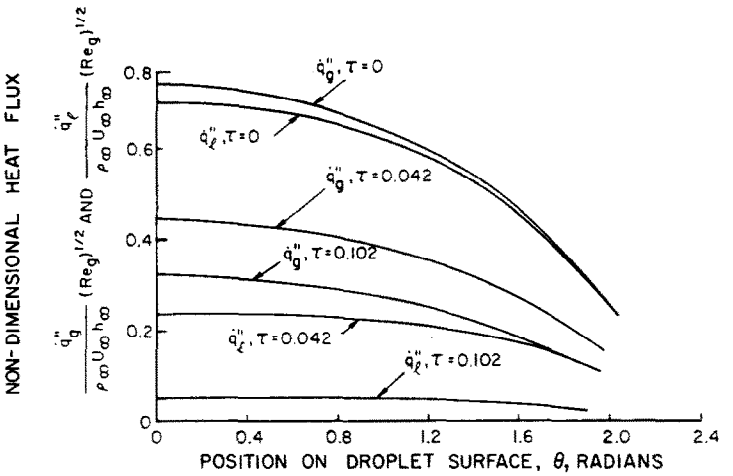

FIG. 8. Heat flux distribution for *n*-decane.

shows the heat flux distribution over the droplet surface at different instants for *n*-decane. As seen from these figures, the heat flux into the liquid phase for hexane is about 7% of the total heat flux on the gas side at the end of the droplet lifetime. For hexadecane 25%, and for decane about 17% of the total heat flux goes into the liquid phase even at the end of the droplet lifetime. The fraction is still larger for all three fuels in the earlier part of their lifetime. This explains the nature of the curves in Figs. 3–6, the more volatile fuel like hexane being closer to a quasi-steady state situation toward the end of the droplet lifetime than the less volatile fuels viz. decane and hexadecane.

A comparison of our results with the Ranz–Marshall type correlation [3] and with the Spalding correlation [4] was made for the vaporization rate. The two correlations are

Ranz–Marshall type correlation

$$\dot{m} = \dot{m}_{ss}(1 + 0.276\, Re_d^{1/2}\, Pr_g^{1/3}),$$

Spalding correlation

$$\frac{\bar{m}'' d}{\mu} = 0.53\, B^{3/5}\, Re_d^{1/2}.$$

In using the above correlations, the heat of vaporization was modified to take into account the heat flux into the liquid phase; the modified heat of vaporization was calculated using our results for the average heat flux into the liquid phase as shown in Fig. 7. The

temporal variation of average mass flux using the above correlations is shown in Figs. 3–5 for the three fuels. A comparison with our results shows that the agreement with the Ranz–Marshall correlation is good during the initial part of the lifetime when the vaporization rate is small. The agreement with the Spalding correlation is better during the later part of the lifetime. It should be noted that the Spalding correlation is suggested for values of B between 0.6 and 5, but the value of B with modification for the liquid-phase heat flux is smaller than 0.6 during the initial part of the lifetime. However, our values towards the end of the lifetime are lower than the values of the two correlations by about 15–20%. This difference could be due to the neglect in our calculations of the wake region which has a bigger contribution towards vaporization when the droplet is heated than in the initial part of the droplet lifetime when it is cold. It should be noted, however, that the Spalding correlation was based on experiments with a gas-phase Reynolds number between 800 and 4000, and the scatter of the experimental results was about 15–20%. The Ranz–Marshall experiments were also conducted for small values of transfer number B. The above comparison suggests that it may be possible to use some empirical correlations like the above two for vaporization rate, if the liquid heat flux is taken into account. However, the calculation of the liquid heat flux would require the solution of the unsteady coupled problem for the gas and the liquid phase.

For a comparison of the droplet lifetime for the three fuels, the curves for $(R/R_0)^{3/2}$ vs τ are plotted on the same graph in Fig. 9. Since the time scale is non-dimensionalized with the thermal diffusion time R_0^2/α_l, the variations in the droplet lifetime for the three fuels are mainly due to the differences in their volatilities; it can be seen from the figure that the variations in the lifetimes for the three fuels are only about 10%, although their volatilities are quite different. However, the vaporization rates in the initial part of the lifetime are substantially smaller for the less volatile fuels, as can be seen from Fig. 9, and this will have significant effect in determining the overall lifetime when considering spray burning in a combustor. In such a situation, there will be a flame front approaching the droplets which are still heating and therefore, the more volatile fuel and the fuel with lower heat of vaporization will have more fuel present to enhance the rate of propagation of the flame front and thereby further increase the rate of vaporization and reduce the overall droplet lifetime. The reason for the small variation in the overall lifetime of a single droplet is that the surface temperature for the less volatile fuel rises quickly to a high value in a very short time during which the quasi-steady thermal boundary layer is established. This time is of $O(Pe_l^{-1}) \cdot R_0^2/\alpha_l$, and is very small and is neglected in the present analysis. This can be seen from Fig. 6 which shows the initial surface temperature to be 346 K for hexane, 384 K for decane, and 428 K for hexadecane. After the initial establishment of the thermal boundary layer, the surface temperature rises quickly initially and then slowly, so that the less volatile fuel is always at a higher temperature at any time, and the droplet lifetime is not significantly affected due to the differences in volatility. Of course, different results can be expected if the ambient gas temperatures were not so high.

Figure 10 shows the temperature distribution inside the thermal core for a decane droplet at various instants. As can be seen from this figure, the droplet temperature becomes uniform only towards the end of the droplet lifetime indicating that the droplet heating is essentially unsteady.

The question arises as to the importance of the

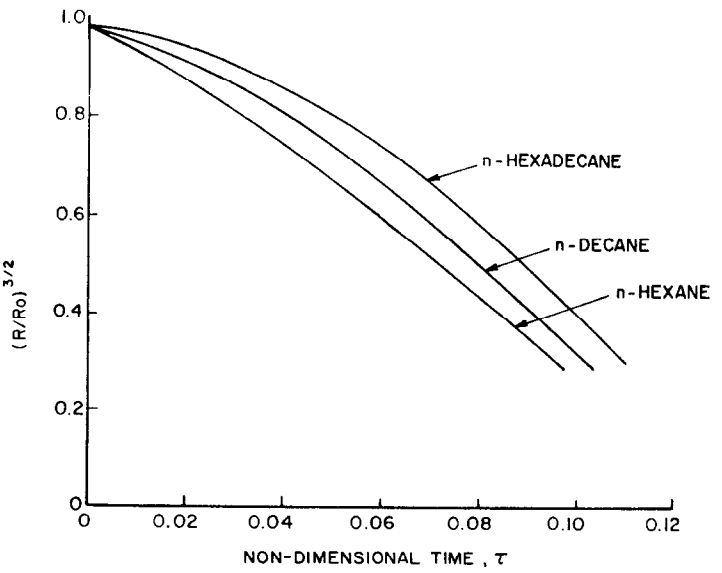

FIG. 9. Results for the three fuels.

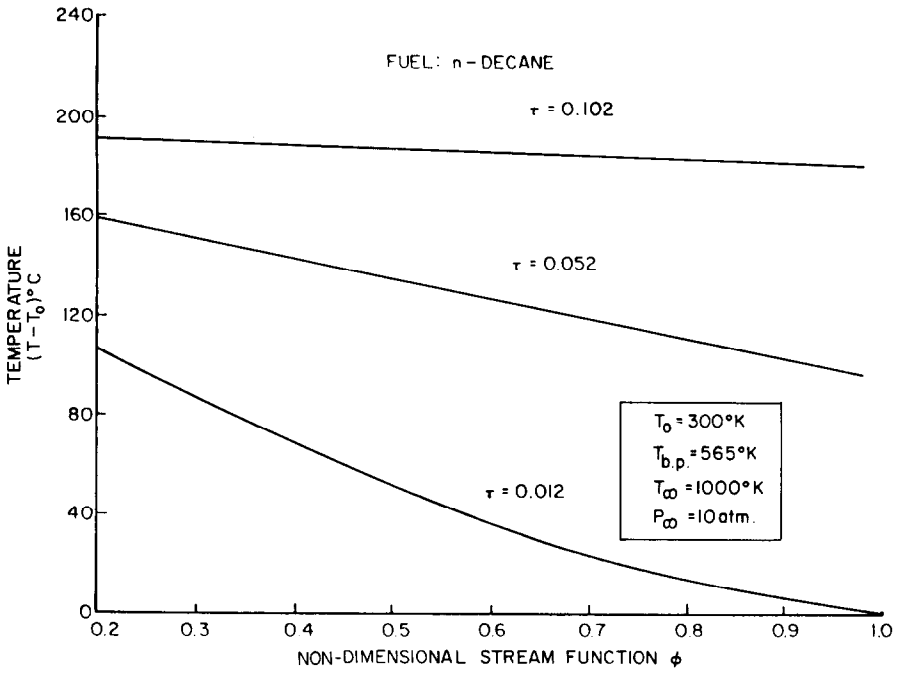

FIG. 10. Temperature distribution inside thermal core.

internal circulation for the droplet vaporization characteristics. The internal circulation model lies between two extreme models: (a) a pure conduction model without any circulation, and (b) a rapid-mixing model. The pure conduction model is a proper limit for zero vortex strength. The rapid-mixing model is the result of faulty reasoning whereby infinite circulation rates are considered to lead to uniform liquid temperature immediately. However, the internal circulation model shows that at large vortex strength, the temperature profile is independent of vortex strength and still nonuniform. Internal circulation leads to a shorter characteristic heating length than in the pure conduction case. In particular, the distance from the droplet surface to the vortex center is a factor of about three less than the droplet radius. This implies that the characteristic heating time (which is proportional to length squared) decreased by about an order of magnitude due to internal circulation. Once the circulation time is short compared to the heating time, the heating time is independent of the circulation time (or essentially independent of the vortex strength). The heating time is defined as the time required to reach a nearly uniform temperature profile in the droplet; it is not necessarily the time required to bring the droplet to a final temperature. In some cases, the droplet temperature will still be increasing at the end of the droplet lifetime. It is expected that the internal circulation via increased heat transfer rates to the droplet interior will yield lower surface temperatures and lower vaporization rates during the initial portion of the droplet lifetime than would be achieved with pure conduction only. The rapid-mixing model should yield still lower vaporization rates during this initial portion.

Less sophisticated models, such as the rapid-mixing model, may give acceptable results for the droplet lifetime. However, in certain situations with moving droplets, an accurate evaluation of the spatial variation of the fuel vapor source strength is required. In such cases, the present type of analysis of the transient phenomenon should be superior.

Summarizing all the above results for an isolated droplet, it can be concluded that the unsteadiness in droplet vaporization persists for most of the droplet lifetime, especially so for the less volatile fuels. The temperature distribution inside the droplet is nonuniform for most of the lifetime; the difference between the surface temperature and the temperature in the interior is higher for the heavier and less volatile fuels. The Ranz–Marshall and the Spalding correlations seem to agree well when the heat flux into the liquid phase is taken into account by modifying the heat of vaporization. The two correlations give higher values for the average mass flux than ours, possibly due to the neglect of the wake region in our calculations.

Acknowledgements — This research has been sponsored by the Department of Energy and the National Science Foundation.

REFERENCES

1. A. Williams, Combustion of droplets of liquid fuels: a review, *Combust. Flame* **21**, 1–31 (1973).
2. W. A. Sirignano and C. K. Law, Transient heating in liquid-phase mass diffusion in fuel droplet vaporization, in *Adv. Chem. Ser. 166, Evaporation-Combustion of Fuels*, Edited by J. T. Zung, American Chemical Society (1978).
3. W. E. Ranz and W. R. Marshall, Evaporation from drops, *Chem. Eng. Prog.* **48**,(3), 141, 173 (1952).
4. D. B. Spalding, Experiments on burning and extinction of

liquid fuel spheres, *Fuel, Lond.* **32**(2), 169–185 (1953).
5. W. A. Sirignano, Theory of multicomponent fuel droplet vaporization. To be published in *Arch. Thermodyn. Combust.*
6. C. K. Law, S. Prakash and W. A. Sirignano, Theory of convective, transient, multicomponent droplet vaporization, in Sixteenth (International) Symposium on Combustion. Combustion Institute, Pittsburgh (1977).
7. S. Prakash and W. A. Sirignano, Liquid fuel droplet heating with internal circulation, *Int. J. Heat Mass Transfer* **21**, 885–895 (1978).
8. N. Frossling, Uber die Verdungtung Fallenden Tropfeu., *Gerlands Beitr. Geophys.* **52**, 170 (1938).
9. S. Prakash, Unsteady theory of droplet vaporization with large gas and liquid Reynolds numbers, Ph.D. Thesis, Princeton University (1978).
10. H. Schlichting, *Boundary Layer Theory*. McGraw-Hill, New York (1968).

THEORIE DE LA VAPORISATION CONVECTIVE DES GOUTTES AVEC TRANSFERT THERMIQUE VARIABLE DANS LA PHASE LIQUIDE

Résumé — On analyse le problème de la vaporisation d'une goutte liquide dans un environnement gazeux convectant. On développe une nouvelle analyse pour une phase gazeuse visqueuse, pour des couches limites de température et de concentration d'espèces, en utilisant une approche intégrale. L'analyse de la phase gazeuse est couplée à une forme modifiée de l'analyse de la phase liquide selon S. Prakash et W. A. Sirignano, *Int. J. Heat Mass Transfer* **21**, 885–895 (1978). Le couplage est résolu pour trois hydrocarbures (*n*-hexane, *n*-décane et *n*-hexadecane). Les résultats montrent que la vaporisation de la goutte est variable et que la distribution de température dans la goutte n'est pas uniforme pendant une grande période de la durée de vie de la goutte. Quelques résultats sont comparés aux relations données antérieurement après les avoir corrigées pour le flux thermique dans la phase liquide.

THEORIE DER KONVEKTIVEN TRÖPFCHENVERDUNSTUNG MIT VERÄNDERLICHEM WÄRMETRANSPORT IN DER ZIRKULIERENDEN FLÜSSIGEN PHASE

Zusammenfassung – Es wird das Problem der Verdunstung von Flüssigkeitströpfchen in eine heiße, gasförmige Umgebung, die sich in Konvektionsbewegung befindet, behandelt. Mit Hilfe einer Integralnäherung wurde für die Beschreibung der Viskositäts-, Wärmeleitungs- und Konzentrationsgrenzschichten der Gasphase ein neues Berechnungsverfahren entwickelt. Die Berechungsmethode für die Gasphase wurde mit einer abgewandelten Form einer früheren Berechnungsmethode für die innere Bewegung und den Wärmetransport in der Flüssigkeitsphase gekoppelt [S. Prakash und W. A. Sirignano, *Int. J. Heat Mass Transfer* **21**, 885–895 (1978)]. Das gekoppelte Problem wurde für drei Kohlenwasserstoff-Brennstoffe (*n*-Hexan, *n*-Decan und *n*-Hexadecan) gelöst. Die Ergebnisse zeigen, daß die Tröpfchenverdunstung unstetig verläuft und daß die Temperaturverteilung innerhalb des Tröpfchens während einer bedeutenden Zeit der Lebensdauer der Tröpfchen ungleichförmig ist. Einige Ergebnisse werden mit den bereits vorhandenen Korrelationen verglichen, nachdem jene zur Berücksichtigung des Wärmestroms in der flüssigen Phase korrigiert wurden.

ТЕОРИЯ КОНВЕКТИВНОГО ИСПАРЕНИЯ КАПЛИ ПРИ НЕСТАЦИОНАРНОМ ПЕРЕНОСЕ ТЕПЛА В ЦИРКУЛИРУЮЩЕЙ ЖИДКОЙ ФАЗЕ

Аннотация — Анализируется проблема испарения жидкой капли в нагретой конвективной газовой среде. С помощью интегрального метода разработан новый способ анализа вязкостного теплового и концентрационного пограничного слоя в газовой фазе. Данный анализ используется совместно с модифицированным анализом для жидкой фазы, предложенным ранее для случая внутреннего движения и теплопереноса [Пракашх и Сиригнано, Международный Журнал Тепло- и Массоперенос, **21**, 885–895 (1978)]. Сопряженная задача решается для трёх углеводородных топлив (*n*-гексан, *n*-декан и *n*-гексадекан). Результаты показывают, что процесс испарения капли является нестационарным, а распределение температур внутри капли — неоднородным в течение бо́льшего промежутка времени существования капли. Проведено сравнение части полученных результатов с имеющимися соотношениями с учётом поправок на тепловой поток в жидкую фазу.